Seasonal constraints on inferred planetary heat content

Karen Aline McKinnon,[1] and Peter Huybers[2]

Corresponding author: Karen Aline McKinnon, Climate and Global Change Division, National Center for Atmospheric Research, Boulder, Colorado, USA. (mckinnon@ucar.edu)

[1]Climate and Global Change Division,
National Center for Atmospheric Research,
Boulder, Colorado, USA.

[2]Department of Earth and Planetary
Sciences, Harvard University, Cambridge,
Massachusetts, USA.

Planetary heating can be quantified using top of the atmosphere energy fluxes or through monitoring the heat content of the earth system. It has been difficult, however, to validate the two methods against each other because of biases in satellite measurements. Here, we focus on the seasonal cycle whose amplitude is large relative to satellite biases. The seasonal budget can be closed through inferring contributions from sparsely sampled high-latitude oceans and marginal seas using the covariance structure of NCAR CESM1. In contrast, if these regions are approximated as the average across observed regions, the amplitude of the seasonal cycle is overestimated relative to satellite constraints. Analysis of the same CESM1 simulation indicates that complete measurement of the upper ocean would increase the magnitude and precision of interannual trend estimates in ocean heating to a greater extent than could be realized through fully measuring the deep ocean.

1. Introduction

Knowledge of the energy imbalance of the planet is critical for the quantification of climate sensitivity, climate model validation, and improved predictions of future warming [*von Schuckmann et al.*, 2016], yet its value remains uncertain. For example, *Loeb et al.* [2012] estimated a global energy imbalance of 0.5 Wm^{-2} and a 90% confidence interval of comparable magnitude at ± 0.43 Wm^{-2}.

Earth's energy imbalance can be inferred through measuring net radiation at the top of the atmosphere (TOA) or monitoring changes in the heat content of the oceans and other elements of the earth system. Ideally these two approaches would offer the opportunity for intercomparison because heating at the TOA must lead to an increase in the heat content of the underlying earth system, but measurement biases and uncertainties make such validation difficult.

The CERES satellite has measured TOA radiation since March 2000 with high precision [within 0.3 Wm^{-2} per decade, *Loeb et al.*, 2007], but the measurements are known to be biased [*Loeb et al.*, 2009], and so do not allow for estimation of the absolute TOA heating rate. Conversely, it is difficult to make spatially and temporally complete measurements of heat content, the majority of which is stored in the ocean [e.g. *Wunsch*, 2016]. Since 2000, Argo floats have improved the sampling of the ocean [e.g., *Lyman et al.*, 2010; *Abraham et al.*, 2013; *von Schuckmann et al.*, 2013], but there remain potentially important measurement gaps in the deep ocean, marginal seas, and at high latitudes (Fig. 1).

Due to the large bias of the CERES measurements and the sparsity of the Argo measurements compared to the volume of the ocean, researchers have combined the best

components of each – the precision of CERES and the mean value from Argo – to obtain better estimates of the TOA energy imbalance [e.g. *Loeb et al.*, 2012]. Satellite measurements, in-situ data, and atmospheric reanalyses have also been used to constrain dynamical ocean models in order to improve estimates of heat content and other ocean properties [e.g., *Wunsch and Heimbach*, 2013; *Balmaseda et al.*, 2013; *Zuo et al.*, 2015]. Such combined estimates have obvious advantages but do not permit for validation across independent methods and datasets.

The agreement between in-situ ocean measurements and TOA radiation has been assessed for interannual variability [*Loeb et al.*, 2012; *Trenberth et al.*, 2016], which is less affected than trend calculations by biases in CERES measurements, but the signal is difficult to identify because the magnitude of interannual variability is comparable to the uncertainty in estimates of ocean heat content.

In contrast, the seasonal cycle is a large, repeated signal that is larger than uncertainties in ocean heat content. Furthermore, estimates of the amplitude and phase of the seasonal cycle in heating measured by CERES are not susceptible to issues of bias in absolute magnitudes that confound estimates of interannual trends. As such, one can independently compare ground and satellite estimates. This comparison demonstrates challenges in closing the planetary energy budget with available measurements and provides a lower bound on the uncertainty in ground-based estimates of planetary heat content.

2. Data

Analysis focuses on the years 2005-2014, spanning the era during which both CERES and Argo data are available, excluding the first five years of Argo when float coverage

was rapidly increasing. While using such a short time period can be problematic for estimating trends, it contains ten iterations of the seasonal cycle and therefore allows for a relatively stable estimate of the seasonality of planetary heat content. TOA radiation measurements are from the CERES satellite [*Wielicki et al.*, 1996]. We use the SYN1deg product at daily resolution. Unlike the higher-order product, EBAF-TOA, the SYN1deg product does not incorporate information from Argo [*Loeb et al.*, 2009].

Ocean temperature measurements are taken from the Scripps gridded product, which relies solely on Argo data. Other direct and indirect sources of information for ocean temperature and heat content do exist, such as instrumented sea mammals [*Roquet et al.*, 2013], ice-tethered buoys [*Toole et al.*, 2011], sea surface temperatures [e.g., *Ishii and Kimoto*, 2009], sea surface height [e.g., *Durack et al.*, 2014; *von Schuckmann et al.*, 2014], moored buoys [*Hayes et al.*, 1991; *Bourlès et al.*, 2008; *McPhaden et al.*, 2009], and reanalyses [e.g., *Zuo et al.*, 2015]. However, because Argo data is currently the largest source of subsurface temperature data and prior estimates of recent ocean heat content trends have often relied solely or primarily on Argo data [e.g., *Lyman et al.*, 2010; *von Schuckmann and Traon*, 2011; *von Schuckmann et al.*, 2013; *Roemmich et al.*, 2015], our ocean analysis also focuses exclusively on Argo data.

Argo trajectories are gridded to $1^\circ \times 1^\circ$ in the horizontal and 58 levels in the vertical using objective mapping in regions where data coverage was viewed as sufficient [hereafter Argo domain, *Roemmich and Gilson*, 2009]. The product spans 60°S – 60°N and does not include the marginal seas (depth $<$ 2000 meters) because few measurements are available in these regions. Due to the exclusion of these regions, the Argo domain is lacking

coverage of 56% of the total ocean volume and 9.5% of the upper 2000 meters. Among the unobserved regions of the upper ocean, two thirds of the volume is in the high latitudes and one third is in the marginal seas. Argo floats do not measure the deep ocean below 2000 meters, although there are efforts underway to deploy floats capable of monitoring such depths [Deep Argo, *Johnson et al.*, 2015].

Energy is also seasonally stored in the atmosphere, land, and cryosphere. Although these reservoirs account for only small contributions to multi-year trends in heat content [*Abraham et al.*, 2013], they have a nontrivial seasonal cycle. The vertically integrated total energy content of the atmosphere – including sensible, latent, potential, and kinetic energy – is based on the ERA-interim reanalysis [*Dee et al.*, 2011] and is calculated using the methods of *Trenberth et al.* [2001]. The heat content of the land surface is estimated using climatological surface temperature data from Berkeley Earth [*Rohde et al.*, 2013] combined with a representation of heat conduction into the solid earth following the approach of *Hansen et al.* [2011]. Arctic sea ice volume is calculated using the Pan-Arctic Ice Ocean Modeling and Assimilation System [PIOMAS, *Zhang and Rothrock*, 2003], and Antarctic sea ice extent is based upon satellite passive microwave data [*Fetterer and Knowles*, 2004]. Antarctic sea ice volume information is not available, so we assume a constant ice thickness of 0.9 meters [*Worby et al.*, 2008]. The seasonal cycle of heat content associated with land ice variations [*Jacob et al.*, 2012] and snow [*Robinson et al.*, 1993; *Willmott et al.*, 1985] are at least an order of magnitude less than the other components, and are neglected.

The physical parameters used to convert measurements of each of the energy reservoirs to units of Joules are in Table 1.

The focus of this work is on estimating the planetary heat content from integrated TOA radiation and surface-based measurements of heat content, but two other approaches are also of note. One is to integrate net energy fluxes at the surface but which is confounded by the sparsity of direct flux observations and the large global imbalances within atmospheric reanalyses [*von Schuckmann et al.*, 2016]. The other is to quantify planetary heating through coupled model simulations that conserve energy [e.g., *Smith et al.*, 2015; *Wild et al.*, 2015] but there remain major questions regarding model bias and representations of external radiative forcing. An expanded analysis of the seasonal cycle of planetary heating based on these approaches may be useful in future work.

3. The seasonal cycle in heat content

The climatological seasonal cycle in TOA radiation from CERES measurements is calculated as the average across 2005-2014. Measurements of radiation are converted to anomalous heat content values at each gridbox through removing the sample mean across the full time series, after which they are integrated across time and the surface area of the earth. Surface area is estimated assuming a spherical planet with a radius of 6371.220 meters and results are reported at monthly resolution. The integration yields a seasonal cycle in planetary heat content that has an amplitude of 2.18×10^{22} J, measured as half the difference between the monthly maximum and minimum of the climatology.

The seasonal cycle deviates slightly from a sinusoid in that planetary heat content decreases more quickly from boreal spring to autumn than it increases from boreal autumn

to spring, likely related to asymmetries in heat capacity between the hemispheres. The peak of the annual cycle of heat content occurs in April, at the end of the Southern Hemisphere summer, consistent with its greater ocean volume. The standard deviation of anomalies across years averages 1.62×10^{21} J across months, or more than an order of magnitude smaller than the amplitude of the seasonal cycle.

In order to compare with the satellite-based estimates, the heat content of the atmosphere, land, cryosphere, and ocean are combined. Among the non-ocean components of the budget, the atmosphere has the greatest amplitude at 8.15×10^{21}J. The maxima of atmospheric energy content occurs in July, shortly after Northern Hemisphere summer solstice, consistent with a small atmospheric heat capacity and greater land mass of the Northern Hemisphere that both heats and provides moisture to the atmosphere (Fig. 2a). The seasonal cycle of land heat content has an amplitude of 4.25×10^{21}J and peaks in September, again reflecting greater Northern Hemisphere land mass. The seasonal cycle of cryospheric heat content is dominated by sea ice variability, and has two maxima during the year, in March and October, because of different phasing of the Arctic and Antarctic. Uncertainty in each component of the heat budget is estimated as the spread of individual years around the ten-year climatology, and uncertainties in their sum are estimated analogously.

The majority of the seasonal cycle in planetary heat content is determined by the seasonal cycle of ocean heat content (Fig. 2a). Because Argo does not measure the highest latitudes, marginal seas, or deep ocean, estimates of planetary heat content using Argo data require implicit or explicit assumptions regarding the relationship between the

heat content of the observed and unobserved regions. We focus on assumptions regarding the marginal seas and high latitudes because the seasonal cycle in heat content is largely confined to the upper ocean. There are a range of methods in the literature for estimating the global integral of heat content from spatially-incomplete data. We focus on the effect of two different assumptions termed the 'Simple Integral' (SI) and 'Weighted Integral' (WI) by *Lyman and Johnson* [2008] that have been used in many prior studies [e.g., *Willis et al.,* 2004; *Levitus et al.,* 2005; *Ishii et al.,* 2006; *Levitus et al.,* 2012 for SI, and *Palmer et al.,* 2007; *Lyman et al.,* 2010; *Roemmich et al.,* 2015; *Cheng and Zhu,* 2015 for WI].

The underlying assumption for the SI method is that the global integral can be calculated as the integral over the available data, or that the mean of the anomaly field in the unobserved regions is zero. In contrast, the WI approach assumes that the observed regions are representative of the unobserved regions. Here, we evaluate the seasonality implied by both methods. The SI-based estimate of heat content is calculated by assuming the anomalies in the high latitudes and marginal seas are zero. Due to the opposite phasing of the seasonal cycles across hemispheres, we calculate the WI-based estimate by infilling missing regions with either the relevant extratropical or tropical (23°S-23°N) volume-weighted average value. Other approaches, such as using smaller regions as representative averages [*von Schuckmann and Traon*, 2011; *Gouretski et al.*, 2012] or using information from sea surface height to infill missing data [*Domingues et al.*, 2008; *Lyman and Johnson*, 2014; *Durack et al.*, 2014] are not considered here.

The amplitude of the seasonal cycle in oceanic heat content in the regions observed by Argo is 3.72×10^{22} J. By construction, the SI approach yields the same value. The WI approach leads to a small increase in the amplitude to 3.85×10^{22} J because a larger volume of the Southern Hemisphere extratropical ocean is infilled than in the Northern Hemisphere, and the seasonal cycle in planetary heat content is in phase with Southern Hemisphere heat content. However, the increase is small because the amplitude of the seasonal cycle in heat content per unit volume in the measured regions is larger in the Northern than Southern Hemispheres (Fig. 2b). The resulting estimates are combined with the non-ocean terms in the heat budget in order to assess closure with respect to the CERES data. In both cases, the inferred planetary heat content has a seasonal cycle that has too large an amplitude compared to the CERES measurements (Fig. 2c).

The misfit using both approaches is primarily due to the lack of measurements in the high latitude Northern Hemisphere waters where the seasonal cycle of heat content has a large amplitude and is of opposite phase to the seasonal cycle of the planetary heat budget. The lack of closure is visually apparent, and is quantified through an examination of the residuals between the CERES-based and infilled estimates. In particular, if the two estimates were consistent, the residuals should not have seasonal structure, which we quantify using the autocorrelation of the residuals at a lag of 12 months. The lag-12 autocorrelation of the SI-based (WI-based) residuals is 0.25 (0.24), which is greater than that expected from Gaussian white noise at the 0.01 level. The distribution of autocorrelations from white noise is calculated using the complementary inverse error function.

Another potential method for statistical infilling of missing ocean data is kriging. We opt not to pursue this approach, however, because the spatial scales of monthly heat content anomalies within Argo are small compared to the distance to new, unobserved regions, especially in the extratropics [*Roemmich and Gilson*, 2009], leading to uncertainties that are larger than the signal. More fundamentally, kriging assumes stationary statistical properties across the domain [e.g., *Cressie*, 1993]. Both the high latitude oceans and the marginal seas are influenced by factors such as the formation of sea ice and bathymetric constraints that are not present in the Argo domain. As such, the assumption of stationarity is unlikely to hold.

Instead, we take advantage of a fully-coupled dynamical model, NCAR CESM1 [*Danabasoglu et al.*, 2012], to provide inference of the covariance structure between the observed and unobserved parts of the ocean, analogous to the approach of *Cheng and Zhu* [2016]. The ocean model within CESM1 is the Parallel Ocean Program version 2 (POP2). In order to match the time span of the observational analysis (2005-2014), a historical simulation is appended to a future simulation forced by the RCP8.5 scenario [*Van Vuuren et al.*, 2011]. The assumption underlying the infilling method is not that CESM1 is properly representing the actual seasonal cycle in heat content, but rather that it can reproduce the correct spatial covariance structure on seasonal timescales.

To perform the CESM1-based infilling, its output is re-gridded to the $1^\circ \times 1^\circ$ grid of the Argo data using a conservative remapping that preserves the global integral of heat. In order to reduce the degrees of freedom in the problem, ocean gridboxes lacking Argo data are grouped together into 126 geographically distinct and contiguous regions, the largest

of which are the polar regions and the Indonesian marginal seas. Regions that span more than 10 degrees of latitude are divided further, yielding 144 total regions whose heat content will be predicted based upon the heat content of gridboxes with measurements (Fig. 1).

The predictive model is trained on the CESM1 output. First, the vertically integrated heat content of each of the 144 contiguous regions is calculated with CESM1. Subsequently, the correlation between the vertically integrated seasonal cycle of heat content in Argo gridboxes and each unobserved region is calculated. Gridboxes having the highest 1% of correlations with a given unobserved region are used for prediction. Prediction coefficients are then obtained through a multiple linear regression constrained to produce only positive coefficients, consistent with the selection criteria for each grid box. Coefficients calculated using the CESM1 output are then applied to the Argo data to obtain a spatially complete estimate of upper ocean heat content.

In order to test the validity of this approach, we randomly remove 144 regions of Argo data of varying size where measurements are available, and estimate the seasonal cycle in the 'missing' regions using the methods outlined in the prior paragraph. The process is repeated 100 times. The time series of the estimated climatological seasonal cycle in heat content has a median correlation with the 'true', or observed, heat content of 0.92, indicating that the annual structure can be reproduced using the covariance structure in CESM1.

The estimated seasonal cycle of heat content in the unobserved regions is in phase with Northern Hemisphere heat content, and therefore of opposite phase from the global

average seasonal cycle of planetary heat content (Fig. 2b). The phasing results from a larger amplitude of seasonal heat storage per unit volume in the Northern Hemisphere than in the Southern Hemisphere – and this effect dominates over the greater Southern Hemisphere ocean volume, unlike in the WI approach. Combining heat content from the infilled and observed regions yields a seasonal cycle of planetary heat content of smaller amplitude that is visually consistent with the CERES data (Fig. 2c). Furthermore, the residuals between the two estimates have a lag-12 month autocorrelation of 0.11, consistent with white noise (p-value = 0.2).

Given the high precision and minimal interannual variability of the TOA radiation measurements of planetary heat content, we infer that the monthly misfits between the two estimates are primarily indicative of uncertainties from measurement and infilling in the ground-based calculation of heat content. The standard deviation of the residuals between the two estimates varies from a minimum of 9.67×10^{21}J in February to a maximum of 1.77×10^{22}J in May. Uncertainty is largest during Southern Hemisphere winter (May through July). Across all months and years, the standard deviation of the residuals is 1.53×10^{22}J. Note that this is a lower bound on the errors because it does not account for uncertainty in the annual mean value of heat content.

4. Importance of marginal and high-latitude seas for decadal heating trends

The analysis of the seasonal cycle highlights the important role of marginal and high-latitude seas for the planetary heat budget. Ocean heat content changes in these regions are not necessarily well represented by the observed regions of the ocean. To explore the

contribution of these regions to the trends in planetary heat content, we again utilize the spatially complete CESM1 simulation.

We first confirm that CESM1 behaves similarly to the observations with regard to the seasonal infilling methods (Fig. 3a). When masked to the Argo domain, the seasonal cycle in ocean heat content is overestimated, and the overestimation is exacerbated using the WI infilling method. Infilling the 'unobserved' regions based on the CESM1 covariance structure produces estimates of seasonal amplitude that are consistent with the values calculated using the full upper ocean, which is unsurprising given that for this check the analysis is self-contained within CESM1. As expected, the amplitude of the seasonal cycle with and without the deep ocean included is very similar.

The trend in ocean heat content between 2005-2014 is calculated using least squares regression on the monthly CESM1 output after the sample climatology has been removed. The trend in CESM1 heat content across the full ocean is 0.58 Wm^{-2} (Fig. 3b). While 0.06 Wm^{-2} of the heating accumulated in the deep ocean below 2000 meters, a total of 0.09 Wm^{-2} accumulated in the high latitudes (0.07 Wm^{-2}) and marginal seas (0.02 Wm^{-2}), despite the fact that these regions only cover 9.5% of the volume of the upper 2000 meters of the ocean.

We do not attempt to infer the magnitude of heating in the high latitudes and marginal seas in the Argo data through infilling via the covariance in CESM1 as was done for the seasonal cycle because we find that neither the seasonal nor interannual covariance structure can skillfully predict decadal trends even within CESM1. We do, however, calculate the inferred heating rate using the WI approach implemented within CESM1,

which leads to an estimate of 0.062 Wm^{-2}, or 69% of the true value, for heating in the high latitudes and marginal seas. This underestimation occurs because high-latitude oceans cover 7% of the volume but account for 14% of the warming of the upper ocean. Of this heat, 60% is in the high Northern latitudes and 40% is in the high Southern latitudes. The situation is analogous to inferences that global surface temperature trends are biased low through assuming Arctic warming rates are proportional to observed regions [c.f., *Cowtan and Way*, 2014]. The marginal seas cover 3% of the volume and account for a proportional 3% of the warming.

We next examine the magnitude of the two primary sources of uncertainty in estimating the planetary heating rate. The first is due to internal variability around the linear trend, and is estimated by first removing the best-fit trend from the data, performing a block bootstrap on the residuals using a block size of one year, adding the best-fit trend back to the bootstrapped residuals, and then re-estimating the trend. The standard deviation of the distribution resulting from iterating the foregoing procedure 10,000 times is used as a metric for trend uncertainty. Uncertainties are similar for the heating rate of the full ocean and only the upper 2000 meters of the ocean at 0.033 Wm^{-2} and 0.032 Wm^{-2}, respectively.

In contrast, a lack of measurements in the marginal seas and high latitudes leads to a 47% increase in the standard deviation of the distribution of heating rates (0.046 Wm^{-2}) compared to the case in which the upper ocean is fully sampled. Increased uncertainty is due to a negative correlation (r = -0.79) in the interannual variability of anomalous heat content in CESM1 between the observed and unobserved regions in the upper ocean,

perhaps due to oceanic heat transport or shifting of fronts. It follows that using the WI approach further increases the uncertainty in the trends to 0.051 Wm^{-2} because the method enforces positive interannual covariance between the observed and unobserved regions – the opposite of what is present in the model. These results indicate that taking measurements in the high latitudes and marginal seas is important for both the precision and accuracy of estimates of oceanic heating rates.

The second source of uncertainty in the trend is due to measurement error. To explore the influence of measurement uncertainty within the context of CESM1, we add noise to the monthly values of planetary heat content that is normally distributed with a standard deviation taken from our estimates of observational uncertainty. Observational uncertainty was calculated as the residual between the TOA seasonal cycle in heat content and the planetary heat content infilled using the covariance structure of CESM1 (see Section 3). Standard deviations are a function of month, though results are similar if the average standard deviation across months is used instead. The spread in the trends induced by errors in measurements and infilling has a standard deviation of 0.028 Wm^{-2}, comparable to the uncertainty due to internal variability when the upper ocean is fully sampled, but smaller than the uncertainty due to internal variability when only the Argo region is sampled within CESM1.

5. Discussion and conclusion

The magnitude of Earth's energy imbalance is one of the most important numbers with respect to understanding climate change [*Trenberth*, 2009; *von Schuckmann et al.*, 2016]. Although measurements of the ocean have improved dramatically in terms of

both their spatial extent and quality in the Argo era, it is not yet clear whether current Argo coverage allows for accurate closure of the planetary energy budget. We focused primarily on the seasonal cycle because high-precision satellite measurements of TOA radiation provide a strong constraint on its amplitude and phase. The seasonal analysis highlights that incomplete sampling of the ocean leads to overestimation of the planetary seasonal amplitude and that this bias is not remedied through assuming that unobserved regions of the ocean can be represented by averages across the observed regions.

Prior estimates of the amplitude of the seasonal cycle in ocean heat content using only ocean data appear to be overestimates compared to satellite constraints [*Antonov et al.*, 2004; *Fasullo and Trenberth*, 2008], presumably due to the same issues with sampling. Using more complex estimates of the covariance structure of heat content from a dynamical model appears sufficient to close the seasonal budget in our analysis.

Examination of the seasonal cycle in planetary heat content also has implications for interannual heating rates. First, interannual heating rate estimates are sensitive to the choice of ocean heat content climatology when sampling is spatially incomplete [*Lyman and Johnson*, 2014; *Cheng and Zhu*, 2015; *Boyer et al.*, 2016]. Given the strong satellite constraint on the seasonal budget, it may be advantageous to determine whether a chosen climatology is consistent with satellite data before using it as the baseline for trend analyses.

Second, the seasonal analysis highlights that regions observed by Argo may be unrepresentative of those that are unobserved. Within CESM1, the volume-weighted ocean heat content has increased faster from 2005-2014 in the high latitudes than in regions observed

by Argo. If the same behavior is evident in the real world, prior estimates of oceanic heating using either the SI or WI approach for infilling [e.g., *Willis et al.*, 2004; *Levitus et al.*, 2005; *Ishii et al.*, 2006; *Levitus et al.*, 2012; *Palmer et al.*, 2007; *Lyman et al.*, 2010; *Roemmich et al.*, 2015; *Cheng and Zhu*, 2015] are underestimates, consistent with recent results that find larger planetary heating rates when sea surface heights [*Durack et al.*, 2014] or data-constrained ocean models [*Trenberth et al.*, 2016] are instead used to infer heat content in regions not observed by Argo. The choice of mapping technique has been identified as the greatest source of uncertainty in trends in ocean heat content [*Boyer et al.*, 2016], so it may be advantageous to assess the different methods on seasonal timescales when the planetary budget is well-constrained by satellite measurements.

Incomplete spatial coverage also increases month-to-month variability in the global integral of heat content within CESM1 because of a negative covariance between the heat content of observed and unobserved regions. This negative covariance likely contributes to the fact that Argo-based estimates of Earth's energy imbalance have considerably more monthly variability than either TOA radiation or ocean reanalyses [*Trenberth et al.*, 2016].

The seasonal heat budget can be closed through combining the covariance structure in CESM1 with observations; however, this method was not applicable for interannual trends because of lack of a satellite constraint and the fact that the covariance structure diagnosed within CESM1 was not generalizable to interannual timescales. Together these results underscore the importance of observing the full upper ocean for purposes of accurately determining Earth's radiative imbalance.

Acknowledgments. The authors thank Kevin Trenberth for his helpful comments. KAM acknowledges NASA NESSF and the NCAR Advanced Study Program for funding. PJH acknowledges NSF grant 1304309. Gridded Argo temperature data is at http://www.argo.ucsd.edu/Gridded_fields.html, PIOMAS Arctic sea ice volume data is at http://psc.apl.uw.edu/wordpress/wp-content/uploads/schweiger/ice_volume/PIOMAS.2sst.monthly.Current.v2.1.txt, Antarctic sea ice extent data is at https://www.ncdc.noaa.gov/snow-and-ice/extent/sea-ice/S/0.csv, vertically integrated atmospheric heat is available at http://www.cgd.ucar.edu/cas/catalog/reanalysis/budgets/index.html, Berkeley Earth temperature data is available at http://berkeleyearth.org/data/, and CESM1 monthly ocean temperature output is available at https://www.earthsystemgrid.org/dataset/ucar.cgd.ccsm4.CESM_CAM5_BGC_LE.ocn.proc.monthly_ave.html.

References

Abraham, J., M. Baringer, N. Bindoff, T. Boyer, L. Cheng, J. Church, J. Conroy, C. Domingues, J. Fasullo, J. Gilson, et al. (2013), A review of global ocean temperature observations: Implications for ocean heat content estimates and climate change, *Reviews of Geophysics*, *51*(3), 450–483.

Antonov, J. I., S. Levitus, and T. P. Boyer (2004), Climatological annual cycle of ocean heat content, *Geophysical Research Letters*, *31*, L04,304.

Balmaseda, M. A., K. E. Trenberth, and E. Källén (2013), Distinctive climate signals in reanalysis of global ocean heat content, *Geophysical Research Letters*, *40*(9), 1754–1759.

Bourlès, B., R. Lumpkin, M. J. McPhaden, F. Hernandez, P. Nobre, E. Campos, L. Yu, S. Planton, A. Busalacchi, A. D. Moura, et al. (2008), The PIRATA Program, *Bulletin of the American Meteorological Society*, *89*(8), 1111.

Boyer, T., C. M. Domingues, S. A. Good, G. C. Johnson, J. M. Lyman, M. Ishii, V. Gouretski, J. K. Willis, J. Antonov, S. Wijffels, J. A. Church, R. Cowley, and N. L. Bindoff (2016), Sensitivity of Global Upper Ocean Heat Content Estimates to Mapping Methods, XBT Bias Corrections, and Baseline Climatologies, *Journal of Climate*, *29*, 4817–4842.

Cheng, L., and J. Zhu (2015), Influences of the choice of climatology on ocean heat content estimation, *Journal of Atmospheric and Oceanic Technology*, *32*(2), 388–394.

Cheng, L., and J. Zhu (2016), Benefits of CMIP5 multimodel ensemble in reconstructing historical ocean subsurface temperature variations, *Journal of Climate*, doi:10.1175/JCLI-D-15-0730.1.

Cowtan, K., and R. G. Way (2014), Coverage bias in the HadCRUT4 temperature series and its impact on recent temperature trends, *Quarterly Journal of the Royal Meteorological Society*, *140*(683), 1935–1944.

Cressie, N. (1993), Statistics for spatial data: Wiley series in probability and statistics, *Wiley-Interscience New York*, *15*, 16.

Danabasoglu, G., S. C. Bates, B. P. Briegleb, S. R. Jayne, M. Jochum, W. G. Large, S. Peacock, and S. G. Yeager (2012), The CCSM4 ocean component, *Journal of Climate*, *25*(5), 1361–1389.

Dee, D., S. Uppala, A. Simmons, P. Berrisford, P. Poli, S. Kobayashi, U. Andrae, M. Balmaseda, G. Balsamo, P. Bauer, et al. (2011), The ERA-Interim reanalysis: Configuration and performance of the data assimilation system, *Quarterly Journal of the Royal Meteorological Society*, *137*(656), 553–597.

Domingues, C. M., J. A. Church, N. J. White, P. J. Gleckler, S. E. Wijffels, P. M. Barker, and J. R. Dunn (2008), Improved estimates of upper-ocean warming and multi-decadal sea-level rise, *Nature*, *453*(7198), 1090–1093.

Durack, P. J., P. J. Gleckler, F. W. Landerer, and K. E. Taylor (2014), Quantifying underestimates of long-term upper-ocean warming, *Nature Climate Change*, *4*(11), 999–1005.

Fasullo, J. T., and K. E. Trenberth (2008), The annual cycle of the energy budget. Part I: Global mean and land-ocean exchanges, *Journal of Climate*, *21*(10), 2297–2312.

Fetterer, F., and K. Knowles (2004), Sea ice index monitors polar ice extent, *Eos, Transactions American Geophysical Union*, *85*(16), 163–163.

Gouretski, V., J. Kennedy, T. Boyer, and A. Köhl (2012), Consistent near-surface ocean warming since 1900 in two largely independent observing networks, *Geophysical Research Letters*, *39*(19), L19,606.

Hansen, J., M. Sato, P. Kharecha, and K. von Schuckmann (2011), Earth's energy imbalance and implications, *Atmospheric Chemistry and Physics*, *11*(24), 13,421–13,449.

Hartmann, L., Dennis (1994), *Global Physical Climatology*, Academic Press, San Diego, USA.

Hayes, S., L. Mangum, J. Picaut, A. Sumi, and K. Takeuchi (1991), TOGA-TAO: A moored array for real-time measurements in the tropical Pacific Ocean, *Bulletin of the American Meteorological Society*, *72*(3), 339–347.

Ishii, M., and M. Kimoto (2009), Reevaluation of historical ocean heat content variations with time-varying XBT and MBT depth bias corrections, *Journal of Oceanography*, *65*(3), 287–299.

Ishii, M., M. Kimoto, K. Sakamoto, and S.-I. Iwasaki (2006), Steric sea level changes estimated from historical ocean subsurface temperature and salinity analyses, *Journal of Oceanography*, *62*(2), 155–170.

Jacob, T., J. Wahr, W. T. Pfeffer, and S. Swenson (2012), Recent contributions of glaciers and ice caps to sea level rise, *Nature*, *482*(7386), 514–518.

Johnson, G. C., J. M. Lyman, and S. G. Purkey (2015), Informing Deep Argo Array Design Using Argo and Full-Depth Hydrographic Section Data*, *Journal of Atmospheric and Oceanic Technology*, *32*(11), 2187–2198.

Levitus, S., J. Antonov, and T. Boyer (2005), Warming of the world ocean, 1955–2003, *Geophysical Research Letters*, *32*(2), L02,604.

Levitus, S., J. I. Antonov, T. P. Boyer, O. K. Baranova, H. E. Garcia, R. A. Locarnini, A. V. Mishonov, J. Reagan, D. Seidov, E. S. Yarosh, et al. (2012), World ocean heat content and thermosteric sea level change (0–2000 m), 1955–2010, *Geophysical Research Letters*, *39*(10), L10,603.

Loeb, N. G., B. A. Wielicki, W. Su, K. Loukachine, W. Sun, T. Wong, K. J. Priestley, G. Matthews, W. F. Miller, and R. Davies (2007), Multi-instrument comparison of top-of-atmosphere reflected solar radiation, *Journal of Climate*, *20*(3), 575–591.

Loeb, N. G., B. A. Wielicki, D. R. Doelling, G. L. Smith, D. F. Keyes, S. Kato, N. Manalo-Smith, and T. Wong (2009), Toward optimal closure of the earth's top-of-atmosphere radiation budget, *Journal of Climate*, *22*(3), 748–766.

Loeb, N. G., J. M. Lyman, G. C. Johnson, R. P. Allan, D. R. Doelling, T. Wong, B. J. Soden, and G. L. Stephens (2012), Observed changes in top-of-the-atmosphere radiation and upper-ocean heating consistent within uncertainty, *Nature Geoscience*, *5*(2), 110–113.

Lyman, J. M., and G. C. Johnson (2008), Estimating annual global upper-ocean heat content anomalies despite irregular in situ ocean sampling*, *Journal of Climate*, *21*(21), 5629–5641.

Lyman, J. M., and G. C. Johnson (2014), Estimating global ocean heat content changes in the upper 1800 m since 1950 and the influence of climatology choice*, *Journal of Climate*, *27*(5), 1945–1957.

Lyman, J. M., S. A. Good, V. V. Gouretski, M. Ishii, G. C. Johnson, M. D. Palmer, D. M. Smith, and J. K. Willis (2010), Robust warming of the global upper ocean, *Nature*, *465*(7296), 334–337.

McPhaden, M. J., G. Meyers, K. Ando, Y. Masumoto, V. Murty, M. Ravichandran, F. Syamsudin, J. Vialard, L. Yu, and W. Yu (2009), RAMA: The research moored array for African-Asian-Australian monsoon analysis and prediction, *Bulletin of the American Meteorological Society*, *90*(4), 459.

Palmer, M., K. Haines, S. Tett, and T. Ansell (2007), Isolating the signal of ocean global warming, *Geophysical Research Letters*, *34*(23), L23,610.

Robinson, D. A., K. F. Dewey, and R. R. Heim Jr (1993), Global snow cover monitoring: An update, *Bulletin of the American Meteorological Society*, *74*(9), 1689–1696.

Roemmich, D., and J. Gilson (2009), The 2004–2008 mean and annual cycle of temperature, salinity, and steric height in the global ocean from the Argo Program, *Progress in Oceanography*, *82*(2), 81–100.

Roemmich, D., J. Church, J. Gilson, D. Monselesan, P. Sutton, and S. Wijffels (2015), Unabated planetary warming and its ocean structure since 2006, *Nature climate change*, *5*(3), 240–245.

Rohde, R., R. A. Muller, R. Jacobsen, E. Muller, S. Perlmutter, A. Rosenfeld, J. Wurtele, D. Groom, and C. Wickham (2013), A new estimate of the average earth surface land temperature spanning 1753 to 2011, *Geoinformatics & Geostatistics: An Overview*, *1*(1).

Roquet, F., C. Wunsch, G. Forget, P. Heimbach, C. Guinet, G. Reverdin, J.-B. Charrassin, F. Bailleul, D. P. Costa, L. A. Huckstadt, et al. (2013), Estimates of the Southern Ocean general circulation improved by animal-borne instruments, *Geophysical Research Letters*, *40*(23), 6176–6180.

Smith, D. M., R. P. Allan, A. C. Coward, R. Eade, P. Hyder, C. Liu, N. G. Loeb, M. D. Palmer, C. D. Roberts, and A. A. Scaife (2015), Earth's energy imbalance since 1960 in observations and CMIP5 models, *Geophysical research letters*, *42*(4), 1205–1213.

Toole, J. M., R. A. Krishfield, M.-L. Timmermans, and A. Proshutinsky (2011), The ice-tethered profiler: Argo of the Arctic, *Oceanography*, *24*(3), 126–135.

Trenberth, K. E. (2009), An imperative for climate change planning: tracking Earth's global energy, *Current Opinion in Environmental Sustainability*, *1*(1), 19–27.

Trenberth, K. E., J. M. Caron, and D. P. Stepaniak (2001), The atmospheric energy budget and implications for surface fluxes and ocean heat transports, *Climate Dynamics*, *17*(4), 259–276.

Trenberth, K. E., J. T. Fasullo, K. von Schuckmann, and L. Cheng (2016), Insights into earth's energy imbalance from multiple sources, *Journal of Climate*, doi:10.1175/JCLI-D-16-0339.1.

Van Vuuren, D. P., J. Edmonds, M. Kainuma, K. Riahi, A. Thomson, K. Hibbard, G. C. Hurtt, T. Kram, V. Krey, J.-F. Lamarque, et al. (2011), The representative concentration pathways: an overview, *Climatic change*, *109*, 5–31.

von Schuckmann, K., and P.-Y. L. Traon (2011), How well can we derive Global Ocean Indicators from Argo data?, *Ocean Science*, *7*(6), 783–791.

von Schuckmann, K., J.-B. Sallée, D. Chambers, P.-Y. Le Traon, C. Cabanes, F. Gaillard, S. Speich, and M. Hamon (2013), Monitoring ocean heat content from the current generation of global ocean observing systems, *Ocean Science Discussions*, *10*, 923–949.

von Schuckmann, K., J.-B. Sallée, D. Chambers, P.-Y. Le Traon, C. Cabanes, F. Gaillard, S. Speich, and M. Hamon (2014), Consistency of the current global ocean observing systems from an Argo perspective, *Ocean Science*, *10*, 547.

von Schuckmann, K., M. Palmer, K. Trenberth, A. Cazenave, D. Chambers, N. Champollion, J. Hansen, S. Josey, N. Loeb, P.-P. Mathieu, et al. (2016), An imperative to monitor Earth's energy imbalance, *Nature Climate Change*, *6*(2), 138–144.

Wielicki, B. A., B. R. Barkstrom, E. F. Harrison, R. B. Lee III, G. Louis Smith, and J. E. Cooper (1996), Clouds and the Earth's Radiant Energy System (CERES): An earth observing system experiment, *Bulletin of the American Meteorological Society*, *77*(5), 853–868.

Wild, M., D. Folini, M. Z. Hakuba, C. Schär, S. I. Seneviratne, S. Kato, D. Rutan, C. Ammann, E. F. Wood, and G. König-Langlo (2015), The energy balance over land and oceans: an assessment based on direct observations and CMIP5 climate models, *Climate Dynamics*, *44*(11-12), 3393–3429.

Willis, J. K., D. Roemmich, and B. Cornuelle (2004), Interannual variability in upper ocean heat content, temperature, and thermosteric expansion on global scales, *Journal of Geophysical Research: Oceans*, *109*(C12).

Willmott, C. J., C. M. Rowe, and Y. Mintz (1985), Climatology of the terrestrial seasonal water cycle, *Journal of Climatology*, *5*(6), 589–606.

Worby, A. P., C. A. Geiger, M. J. Paget, M. L. Van Woert, S. F. Ackley, and T. L. DeLiberty (2008), Thickness distribution of Antarctic sea ice, *Journal of Geophysical Research: Oceans*, *113*(C5).

Wunsch, C. (2016), Global ocean integrals and means, with trend implications, *Annual review of marine science*, *8*, 1–33.

Wunsch, C., and P. Heimbach (2013), Dynamically and kinematically consistent global ocean circulation and ice state estimates, in *Ocean Circulation and Climate: A 21 Century Perspective*, edited by G. Siedler, S. M. Griffies, J. Gould, and J. A. Church, pp. 553–579, Academic Press, Oxford, UK.

Zhang, J., and D. Rothrock (2003), Modeling global sea ice with a thickness and enthalpy distribution model in generalized curvilinear coordinates, *Monthly Weather Review*, *131*(5), 845–861.

Zuo, H., M. A. Balmaseda, and K. Mogensen (2015), The new eddy-permitting ORAP5 ocean reanalysis: description, evaluation and uncertainties in climate signals, *Climate Dynamics*, pp. 1–21, doi:10.1007/s00382-015-2675-1.

Table 1. Values of parameters used to convert measurements to Joules.

Parameter	Value	units	Reference (if applicable)
Heat capacity of water	3990	J kg^{-1} K^{-1}	*Fasullo and Trenberth* [2008]
Density of ocean water	1026.5	kg m^{-3}	*Fasullo and Trenberth* [2008]
Density of ice	917	kg m^{-3}	
Latent heat of fusion	3.34×10^{-5}	J kg^{-1}	
Diffusivity of land	5×10^{-7}	m^2 s^{-1}	*Hartmann* [1994]
Volumetric heat capacity of land	2.5×10^{6}	J m^{-3} K^{-1}	*Hartmann* [1994]

Figure 1. Data availability from Argo. Light blue regions are sampled sufficiently well to produce gridded estimates of temperature via objective mapping [*Roemmich and Gilson*, 2009]. Colored and white regions in the ocean are not observed by Argo. The colors show the largest 25 contiguous regions used for inferring heat content based upon the covariance structure in NCAR CESM1. The white regions show the remaining 119 regions that are also infilled. For the full ocean, floats do not measure below 2000 meters.

Figure 2. The seasonal cycle of planetary heat content. (a) The seasonal cycle of each component of planetary heat content. The vertical bars show one standard deviation of the year-to-year variability for each month, and the dots indicate the mean value across all years. The year-to-year variability for the land, atmosphere, and cryosphere is small on the scale of the plot. (b) The seasonal cycle of heat content estimated for the regions unobserved by Argo. (c) The seasonal cycle in planetary heat content calculated from CERES measurements (red) as compared to estimates using various infilling methods. The SI (green) and WI (yellow) methods yield a seasonal cycle with too large an amplitude. Infilling based on the covariance structure in CESM1 (purple) yields estimates consistent with CERES.

Figure 3. The seasonal cycle and trends in ocean heat content within CESM1 for 2005-2014. (a) The amplitude of the seasonal cycle based upon different masking and infilling strategies. The distributions are estimated through re-sampling years with replacement 10,000 times before calculating the climatology. (b) Trends in ocean heat content. The sample climatology is removed before trends are calculated. The distributions are estimated through a bootstrapping procedure wherein the best-fit trend line to the data is removed, the residuals are randomly sampled with replacement 10,000 times and added back to the best-fit trend line, and then a new trend line is calculated. The process assumes that the residuals are interchangeable after the seasonal cycle and trend are removed.

Figure 1. Figure

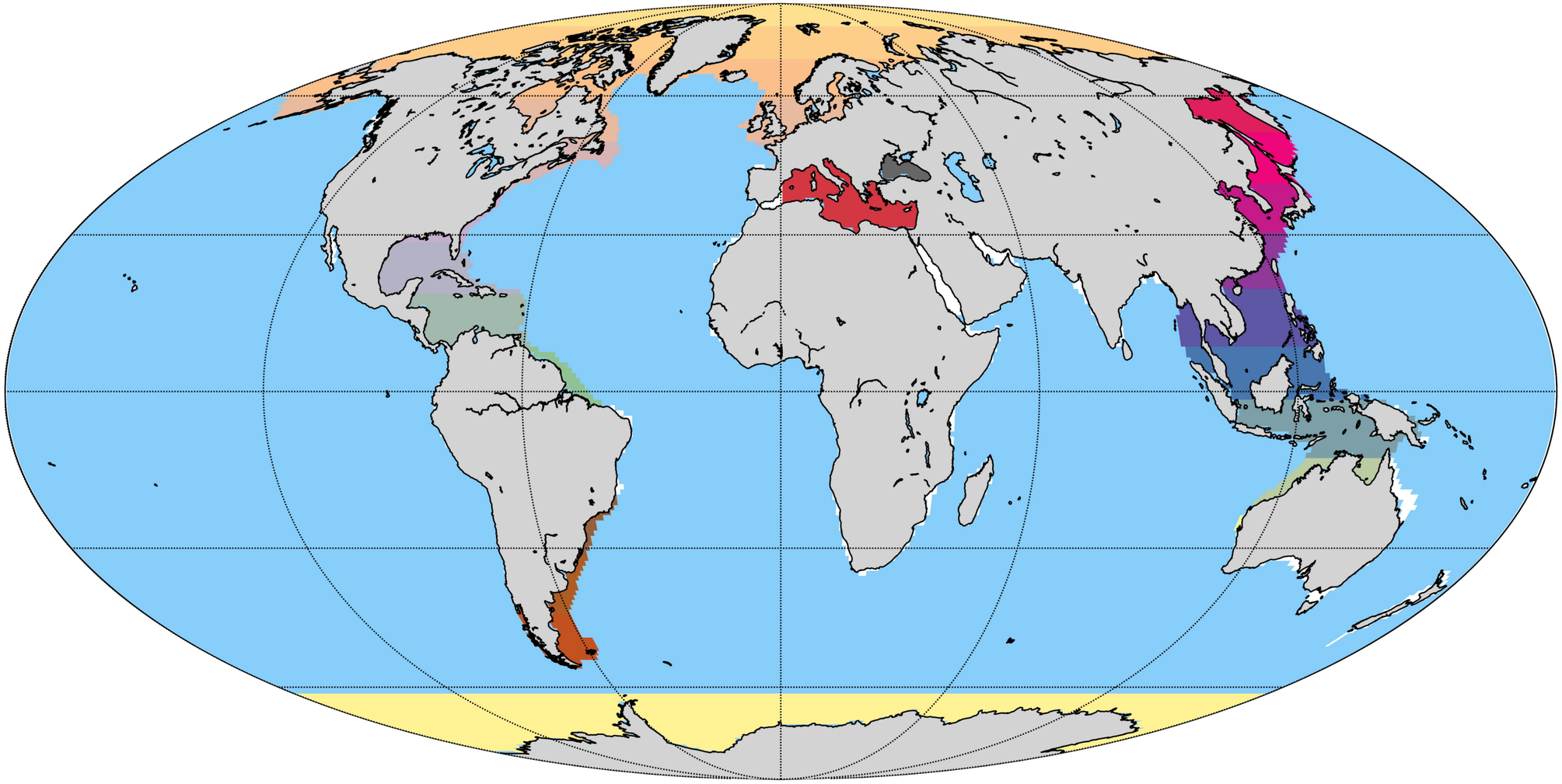

Figure 2. Figure

Atmosphere
Land
Cryosphere
Ocean

Heat anomaly (10^{22} J)

SI
WI
CESM cov

Heat anomaly (10^{22} J)

SI total
WI total
CESM cov total
CERES

Heat anomaly (10^{22} J)

Month

Figure 3. Figure

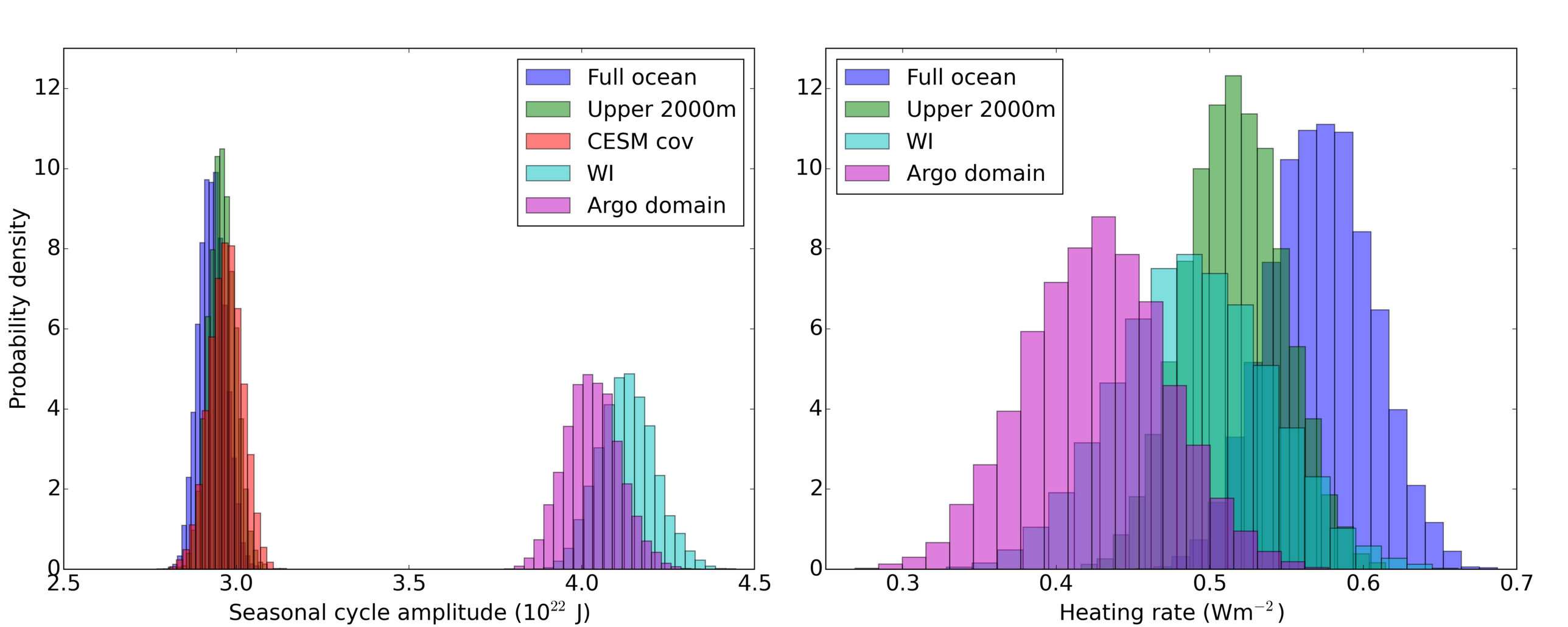
Full ocean
Upper 2000m
CESM cov
WI
Argo domain
Probability density
Seasonal cycle amplitude (10^{22} J)
Full ocean
Upper 2000m
WI
Argo domain
Heating rate (Wm^{-2})